

Optical methods to characterise the composition and homogeneity of lithium niobate single crystals

M. Wöhlecke¹, G. Corradi², K. Betzler¹

¹ FB Physik, Universität Osnabrück, D-49069 Osnabrück
(Fax: +49-541/9692670, E-mail: manfred.woehlecke@physik.uni-osnabrueck.de)

² Research Lab. for Crystal Physics, HAS, P.O.Box 132, Budapest, H-1502, Hungary

Received: 28 March 1996 / Accepted: 8 June 1996

Dedicated to O. F. Schirmer on the occasion of his 60th birthday

Abstract. A number of the physical properties of lithium niobate strongly depend on sample composition. Although several procedures for the determination of the composition have already been published, a critical survey and an introduction to standard methods recommendable also for laboratories active in R&D of LiNbO₃ devices is still missing. Within a detailed description of a series of methods, we summarise their capabilities and accuracy. The proposed optical characterisation methods, in particular those based on the generation of second harmonic light and those involving the measurement of birefringence and the UV absorption edge are found to be most convenient for an accurate and fast standard characterisation of LiNbO₃ single crystals. An absolute accuracy of 0.1 mol% based on a comparison with the Curie temperature calibration method and a relative accuracy of up to 0.01 mol% are available. Some of these methods are also suited for the two or three dimensional homogeneity control of LiNbO₃ single crystals.

PACS: 78.20.-e; 77.84.Dy; 81.70.-q

Lithium niobate is a well-known ferroelectric material exhibiting strongly coupled acousto- and electro-optical properties and non-trivial defect structures, for reviews see [1, 2, 3, 4]. LiNbO₃ is one of the most promising materials for integrated optics devices and optical computers [5, 6].

A basic problem limiting most applications is the control of the composition and homogeneity in single crystals. The solid solution range of the Li₂O - Nb₂O₅ system extends from 46 to 50 mol% Li₂O at 1000 °C and from 48 to 50 mol% Li₂O at room temperature [7, 8]. Single crystals of best quality and uniform composition have been grown for the congruent composition (at about 48.4 mol% Li₂O), using the Czochralski technique. Most crystals used for investigations and applications are congruent ones. Crystals grown from other Li-deficient, stoichiometric or Li-surplus melts have compositions differing from that of the melt, with the composition changing strongly along the growth direction. Several attempts have been made to overcome this problem. A straightforward one is the use of continuous refill or double crucible Czochralski methods to maintain a fixed composition [9, 10]. Recently new procedures for preparing

LiNbO₃ crystals with compositions very close to stoichiometric material have been devised, opening new perspectives for applications. Floating zone techniques, in conjunction with point heating can enforce non-congruent compositions for crystal fibers, as e.g. in the laser heated pedestal growth method [11]. Similar methods using an ellipsoidal mirror can be used for the preparation of crystal fibers with any desired composition in the range 47–49.8 mol% Li₂O [12]. In the vapour transport equilibration (VTE) method, which is a post-growth technique, a crystal with congruent composition is annealed in a Li-rich atmosphere [13, 14]. With regard to single crystals the method using the addition of potassium to the melt is even more promising [15, 16]. In contrast to most other dopants nearly all potassium remains in the melt, thus only 'catalysing' stoichiometric growth. In the meantime at least two crystal growth laboratories (Ashtarak, Budapest) have repeatedly grown samples with a Li₂O content of more than 49.9 mol% in the bulk utilizing this method.

Similarly to improved stoichiometry some dopants introduced in concentrations above a given threshold also alter intrinsic properties. The effect of Mg on the photorefractive behaviour [17] with a threshold of about 5.5 mol% was the first example found. Another divalent dopant with a less sharp threshold near 7 mol% is Zn [18]. Examples for trivalent dopants are In [19], and Sc [20] with a much lower threshold value of about 1–2 mol%.

Most papers dealing with LiNbO₃ do not give complete and reliable information on composition and purity of the crystal samples used, strongly impeding comparisons and general conclusions. Due to controversial opinions and preferences, and lacking reliable, generally trusted calibration curves, such a characterisation still remains a rather hard task. Therefore a community of laboratories involved in LiNbO₃ research and united by a Network of the European Science Foundation undertook a joint effort to make a critical summary of earlier results, to define clear preferences for the methods of characterisation, and to present new reliable and widely controlled calibration data for a few preferred methods. Such recommendations are thought to be helpful for a standard characterisation of LiNbO₃ crystals in the future, facilitating their applications. The present state of this task is summarised in this paper.

1 Non-optical methods for the characterisation of the composition

1.1 Chemical analysis

Destructive analyses using acidic decomposition and chromatographic [21] or atomic absorption analysis [12] or inductively coupled plasma atomic emission spectroscopy (ICP-AEA) [22] for determining the Li, and gravimetry to measure the Nb content [23], require rather large sample quantities, are lengthy, tedious, subject to systematic errors and offer a precision of at most 0.2 mol% [12, 22].

1.2 Melt composition

The crystal composition does not uniquely depend on the melt composition, as geometrical and other growth parameters strongly influence the growth process, even if continuous refill is used. Curves obtained for such a dependence (e.g. the one obtained by Carruthers et al. [24] or Furukawa et al. [22]) have therefore only qualitative significance and can be described by the following empirical equation

$$c_{\text{Li}} = 48.5 + 0.3436(c_{\text{Li,melt}} - 48.5) - 0.02897(c_{\text{Li,melt}} - 48.5)^2 \quad (1)$$

derived from experimental data published in several reports [22, 24, 25], c_{Li} and $c_{\text{Li,melt}}$ denoting the Li_2O content in mol% of the bulk and melt, respectively. The equation is valid in the range $45 < c_{\text{Li,melt}} < 52$ mol% Li_2O with an accuracy of 0.3 mol% provided that the growth conditions do not differ strongly from those in the cited reports.

1.3 Measurement of the Curie temperature

The Curie temperature has been found to change linearly by roughly 150 °C in the solid solution range [24], which provides sufficient sensitivity for composition measurements, however the high T_c close to the melting point is a major drawback of this method. DTA measurements on four single crystals characterised by chemical analysis have been recently carried out by Iyi et al. [12]. These results, obtained in the 47 - 49.8 mol% region, show a linear dependence of the Curie temperature on the Li_2O content c_{Li} and can be summarised by the fit

$$T_c = 39.26 c_{\text{Li}} - 760.67 \text{ or} \\ c_{\text{Li}} = 0.02546 T_c + 19.39 \quad (2)$$

where T_c is the Curie temperature in centigrades. Bordui et al. [26] obtained a similar fit for five VTE equilibrated single crystals in the composition region 47 - 49.6 mol% using dielectric measurements:

$$T_c = 39.064 c_{\text{Li}} - 746.73 \text{ or} \\ c_{\text{Li}} = 0.02557 T_c + 19.149 \quad (3)$$

The composition of each crystal sample was assumed to be identical with that of the single-phase powder used for its VTE equilibration. This was checked by measuring T_c for

both the crystal and the powder in each case. The absolute accuracy of the T_c measurement was estimated to be 0.3 and 0.6 °C for single crystals and powders respectively, the powder compositions were defined within 0.01 mol%. The reproducibility of crystal composition values obtained by VTE processing was checked near the congruent point in a previous paper of the same group [27] where the authors determined the congruent composition with high precision (48.38 ± 0.015 mol%) and showed that crystal samples with appreciably differing compositions can be made congruent by VTE processing them in a powder charge of congruent composition. So Bordui et al. [26] claim a higher precision for c_{Li} than Iyi et al. [12]. Now, Eqs. (2) and (3) yield results differing only by 4 °C or $\Delta c_{\text{Li}} = 0.1$ mol%, which is only half of the absolute error for c_{Li} estimated by Iyi et al. [12]. For these reasons we favour the second calibration (3) and think that an absolute accuracy of 0.1 mol% is realistic. It should be mentioned, however, that earlier measurements on similar powders gave systematically lower T_c values [28, 29], the deviations being of the order of 10 °C which is several times the standard deviations of those measurements. The reason for this discrepancy is unknown.

For compositions very close to the stoichiometric one the Curie point is higher than the melting point. As claimed by Gallagher and O'Bryan [30], in this range mechanic dilatometric measurements of T_c are still possible, their result of 1198 °C obtained on a single crystal VTE equilibrated with stoichiometric powder is again lower than 1202 or 1206 °C expected from (2) and (3), respectively. The deviation from linearity in the nearly stoichiometric range reported by Grabmaier [31] has not been confirmed.

Impurities are known to modify the Curie temperature of LiNbO_3 substantially. The addition of 1 mol% Mg to ceramic samples from 47 to 50 mol% Li_2O results in a uniform increase of T_c by 22 °C [24]. For Mg concentrations near 5 mol% the increment saturates with a value of about 60 °C [28]. The addition of Ti on the other hand results in a 9 °C/mol% decrease of T_c up to 20 mol% [29].

The DTA and the related more powerful DSC method require powdered samples of the order of 0.5 and 0.01 g respectively. For dielectric measurements single crystals or pellets of moderate sizes (e.g. $4 \times 6 \times 1$ mm³) and for dilatometric methods single crystal prisms (e.g. $6 \times 2 \times 2$ mm³) have been used.

Measurements of the melting temperature for the given purpose are less feasible due to smaller precision and other evident reasons.

1.4 Density measurements

The density of LiNbO_3 was found to change only by $1.5 \cdot 10^{-2}$ g/cm³ over the solid solution range while the experimental error of density measurements is normally $3 \cdot 10^{-3}$ g/cm³ [7, 12, 32, 33]. The precision of the measurement had to be increased by at least an order of magnitude if the method was to be used for calibration.

1.5 Diffraction methods

The lattice constants of LiNbO₃ show an appreciable decrease with increasing Li content. Recently X-ray and neutron diffraction measurements in the range 47 - 49.8 mol% Li₂O content have been carried out by Iyi et al. [12] and an overall decrease of 0.004 Å and 0.014 Å for the lattice constants *a* and *c*, respectively, has been found. The dependences of these constants on the Li content seem to be less linear than that of the unit cell volume. Using the powder data of Iyi et al. [12], taken at room temperature, for the volume of the hexagonal unit cell $V = \sqrt{3}a^2c/2$ the following linear fit can be given

$$V = 334.7 - 0.3338c_{\text{Li}} \quad \text{or} \quad c_{\text{Li}} = 992.8 - 2.965V \quad (4)$$

where *V* is in Å³. There is a small discrepancy between X-ray and neutron diffraction measurements [12, 34] limiting the confidence in such a calibration to 0.2 - 0.3 mol%. This value is further increased by the uncertainty of the composition data and the possible deviations from linearity, resulting in an estimated precision of 0.3 - 0.4 mol%. The dependence of *V* on impurity content is much weaker than on the changes of the Li content, Mg increases, while K induces a decrease of the lattice constants [35]. The measurements require very small amounts (less than 1 mm³) of sample material.

1.6 Linewidth of NMR and EPR signals

The width of the ⁹³Nb NMR line was used as early as 1969 by Peterson and Carruthers [36] for the characterisation of the stoichiometry of LiNbO₃ powders. The halfwidth of the low-field derivative line was found to decrease from 26 to 8 Gauss for a change from 48 to 50 mol% of the Li₂O content (for a measurement at 19.24 MHz at room temperature) and did not change outside the single phase range. No comparable single crystal study has been carried out. A general problem with NMR calibration is expected to remain due to background paramagnetic impurities and random internal strain fields contributing to the linewidth, even for the presently available higher magnetic fields and rotational techniques [37].

The narrowing of EPR lines of background Fe impurities, upon approaching the stoichiometric composition, has been investigated by Malovichko et al. [16, 38] in the X band for four compositions in the 48.5 - 50 mol% Li₂O range. The EPR lines of even a few ppm of Fe can be detected, especially for nearly stoichiometric crystals. The dependence on composition appeared to be linear if the Fe concentration was smaller than 0.01 mol%. In this case, for room temperature, the linewidth of e.g. the transition at 60 mT for the magnetic field perpendicular to the *c* axis decreased from 22 to 4 mT; at low temperature, 14 K, the transition at 300 mT for the same orientation was found to narrow from 46 to 4 mT upon approaching the stoichiometric composition. Assuming reproducibility of the data this method could discern composition changes of at about 0.25 mol% at room temperature and 0.1 mol% at low temperatures. The samples required for the measurement have to be single crystals with known *c* direction and a volume preferably between 20 and 50 mm³.

1.7 Velocity of surface acoustic waves

The elastic properties of LiNbO₃ single crystals and in particular the velocity of surface acoustic waves (SAW) also depend on composition. An increase of 37 m/s/mol% of the SAW velocity has been observed for 128° XY cuts near the congruent composition checked by the Curie method [39]. The relative precision of the method was claimed to be of the order of 0.01 mol%. However, other measurements on similar cuts containing 47.5 - 49 mol% Li₂O [40] yielded values shifted by some 50 m/s stressing the need of more stringent control of experimental circumstances like orientational precision, thermal treatments, surface contamination etc. The method may be straightforward for composition control in device development where similar cuts are used and standard procedures for preparing the surface contacts are available.

1.8 Ion beam methods

Rutherford backscattering, channeling, proton-induced X-ray absorption and related ion beam methods have been helpful for finding the substitution sites of a number of impurities, however, the separation of contributions of various atoms cannot be carried out with the precision required for composition measurements.

2 Optical methods for the characterisation of the composition

2.1 Measurement of the UV absorption edge

The position of the fundamental absorption edge is very sensitive to the composition of LiNbO₃. Földvári et al. [41] found a blue shift from 320 to 311 nm upon moving from 48.6 mol% towards a near stoichiometric composition. The position of the band edge was defined as the wavelength where the absorption coefficient is 20 cm⁻¹. A further large shift to the blue has been observed in crystals prepared by the VTE method or in a potassium doped melt [16]. The band edge wavelengths in the latter work are given for the absorption coefficient 15 cm⁻¹.

Although the relationship is non-linear, the measurement of the UV absorption edge would be a very convenient way for characterising the crystal composition. Therefore the laboratories of the authors started an extensive study of the absorption edge combined with cross-checking using SHG-based methods. The details will be reported elsewhere. Here we show the main results and present an equation describing the band edge as a function of composition in the bulk. First we point out that the two sample surfaces crossed by the light beam should be polished to a moderate optical quality with a density of scratches less than 1% of the total area. The orientation of the crystal is not critical, better than five degrees are sufficient. A correction for the reflection is necessary shifting the edge by about one nm to the blue. For the convenience of the reader two equations are given, one for 15 and one for 20 cm⁻¹. Above 49.5 mol% Li₂O the sensitivity is high, mapping a change of 0.1 mol% to 2 nm.

Thus even non-sophisticated spectrometers allow a moderate accuracy, high resolution instruments 0.02 mol%. The absolute uncertainty of the calibration curve is that of the underlying Curie-temperature determination, i.e. 0.1 mol%.

$$\lambda_{15} = 321.9 - 1.597x - 5.745x^2 \quad \text{at } 15 \text{ cm}^{-1} \quad (5)$$

$$\lambda_{20} = 320.4 - 1.829x - 5.485x^2 \quad \text{at } 20 \text{ cm}^{-1} \quad (6)$$

The variable x is the deviation from the congruent composition (48.38 mol%) in mol%. It should be pointed out that Eqs. (5) and (6) are valid for light being polarized parallel and propagating perpendicular to the polar c axis.

2.2 Measurement of the refractive indices

2.2.1 Sellmeier equation and direct evaluation

Lithium niobate exhibits a negative birefringence and its index ellipsoid depends in a characteristic way on the composition.

The up to now most careful study of the refractive indices covering the whole composition range of lithium niobate has been carried out by Schlarb et al. [42] who used an interferometric method for the measurements. The experimental results can be approximated by a generalised Sellmeier equation for the wavelength and composition dependence of the refractive indices

$$n_i^2 = \frac{A_{0,i} + A_{1,i}(50 - c_{\text{Li}})}{\lambda_{0,i}^{-2} - \lambda^{-2}} + A_{\text{UV}} - A_{\text{IR},i}\lambda^2 \quad (7)$$

where λ is the wavelength measured in nm and c_{Li} the Li content in mol%. The intensity factors A describe the influence of the various oscillators (optical transitions) responsible for the refractive indices in the visible and near infrared region – A_0 : Nb on Nb site, A_1 : Nb on Li site, A_{UV} : remaining oscillators at higher energy (transitions to higher energetic states in the conduction band, plasmons etc.), A_{IR} : phonons. The parameters are listed in Table 1 for the ordinary and the extraordinary refractive indices ($i = o, e$), respectively.

This Sellmeier equation is valid in a composition range $c_{\text{Li}} = 47 \dots 50$ mol% and a wavelength range $\lambda = 400 \dots 3000$ nm. Experimental index of refraction data are described with an error less than 0.002.

Direct measurements of the refractive indices (preferably of n_e which depends much stronger on c_{Li}) in conjunction with (7) can be used for determining the composition of crystal samples. For all methods described in Sects. 2.2–2.4 samples with two polished surfaces and a minimum light path of 2–3 mm are needed.

2.2.2 Birefringence

In general it is more convenient to measure the birefringence $\Delta n = n_e - n_o$ of a crystalline sample than to measure the refractive indices directly. Furthermore, as n_o varies only slightly as a function of composition, the composition dependent relative variation of Δn exceeds that of n_e by a factor of $n_e/\Delta n \approx 25$. For the application of birefringence

Table 1. Parameters for the generalized Sellmeier equation (room temperature values)

Parameter	$n_o (i = o)$	$n_e (i = e)$
$A_{0,i}$	4.5312×10^{-5}	3.9466×10^{-5}
$A_{1,i}$	-4.8213×10^{-8}	7.9090×10^{-7}
$\lambda_{0,i}$	223.219	218.203
$A_{\text{IR},i}$	3.6340×10^{-8}	3.0998×10^{-8}
A_{UV}	2.6613	2.6613

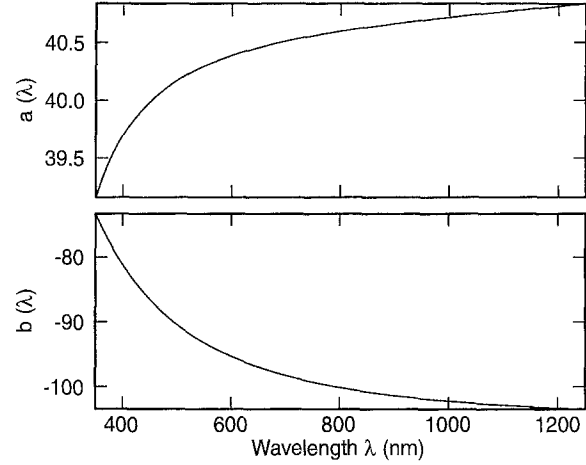


Fig. 1. Wavelength dependence of the parameters a and b at room temperature (see text)

measurements an approximately linear correspondence between Li content c_{Li} and birefringence Δn can be derived from (7) [25]:

$$c_{\text{Li}} = a(\lambda) + b(\lambda) \Delta n. \quad (8)$$

The wavelength dependence of the parameters a and b is sketched in Fig. 1. For the wavelength of a HeNe laser (633 nm), which often is available for such measurements, the parameters are $a = 40.43$ and $b = -96.4$. Applying (8), one has to bear in mind that for LiNbO_3 $\Delta n < 0$.

2.3 Colinear optical frequency doubling

Optical second harmonic generation (SHG) measurements provide indirect albeit very accurate techniques for the characterisation of electrooptic materials. All of these techniques use phase matching between the fundamental and the generated second harmonic beam which means that momentum conservation is fulfilled for this process or – for colinear SHG – that fundamental and harmonic beam experience equal refractive indices. The methods thus profit from the sensitivity enhancement imposed by the detection of the vanishing difference between two refractive indices. Usually a Q-switched Nd:YAG laser provides the necessary fundamental beam.

2.3.1 Phase matching temperature for second harmonic generation

One of the most common methods is to measure the phase matching temperature T_{PM} for doubling Nd:YAG laser light

using so-called noncritical phase matching. A fundamental laser beam with ordinary polarization generates extraordinarily polarized second harmonic light, both wave vectors pointing perpendicularly to the polar axis of the crystal. The two involved refractive indices show different temperature dependences, phase matching is achieved by temperature tuning.

T_{PM} strongly depends on the crystal composition and thus can be used as a measure for the characterisation of the stoichiometry. The dependence – calculated from a temperature dependent Sellmeier equation [43] – is depicted in Fig. 2 together with several experimental data. T_{PM} can be measured with an accuracy usually better than 1 K yielding a theoretical sensitivity of better than 0.01 mol% for the composition determination.

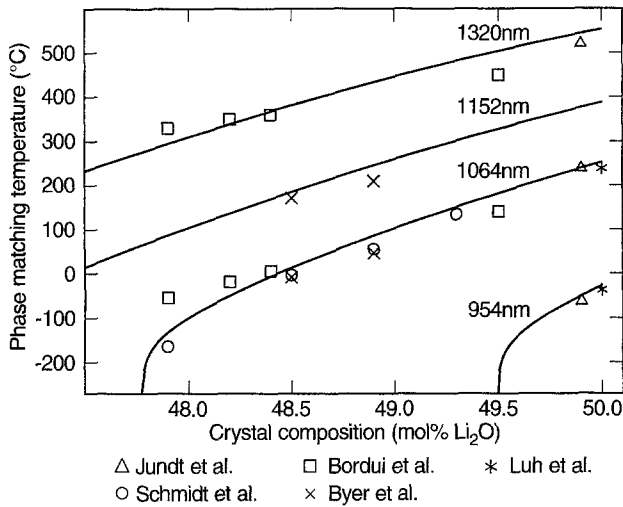


Fig. 2. Calculated phase matching temperature of LiNbO_3 as a function of the Li content in the crystal for various fundamental wavelengths. Data points are experimental values from several other authors [14, 26, 11, 44, 45]

2.3.2 Phase matching angle for second harmonic generation

Instead of using temperature tuning, phase matching can be achieved by angle tuning: the crystal has to be rotated around an axis perpendicular to both the polar axis of the crystal and the beam direction. The effective extraordinary refractive index depends on the rotation angle, the angle at which the phase matching condition is fulfilled characterises the composition [43].

2.4 Noncolinear optical frequency doubling

In the case of colinear frequency doubling (see Sect 2.3) the wave vectors of the interacting light waves are parallel to each other. The phase matching condition (i. e. momentum conservation for the interacting photons) is fulfilled in a quasiscalar way for the wave vectors of the fundamental ($\mathbf{k}_1, \mathbf{k}'_1$) and the generated harmonic wave (\mathbf{k}_2):

$$|\mathbf{k}_1| + |\mathbf{k}'_1| = |\mathbf{k}_2|. \quad (9)$$

When using noncolinear frequency doubling, where the two fundamental wave vectors are inclined to each other, a vectorial phase matching condition has to be obeyed:

$$\mathbf{k}_1 + \mathbf{k}'_1 = \mathbf{k}_2. \quad (10)$$

The doubling geometry (i. e. the angle between the two fundamental beams) then can be used as an additional or even only tuning parameter to characterise the material.

2.4.1 Spontaneous noncolinear frequency doubling

In a spontaneous noncolinear frequency doubling arrangement (SNCFD) laser light is directed onto the sample in a direction perpendicular to the optical axis of the crystal, the second of the two necessary fundamental waves is provided by randomly scattered laser light. The interaction between the intense laser beam and the scattered waves results in a cone of generated second harmonic light with a cone angle characteristic for the composition of the investigated sample [46, 47]. The cone angle is determined by the refractive indices of the material thus can be calculated using the generalized Sellmeier equation (7). For a fundamental wavelength of 1064 nm (Nd:YAG laser) the composition of the sample is in good approximation described by

$$c_{\text{Li}} = 48.528 + 0.0013 \cdot \varphi' + 0.00625 \cdot \varphi'^2, \quad (11)$$

where c_{Li} is measured in mol% and $2 \cdot \varphi'$ is the full cone angle measured in the plane perpendicular to the polar axis outside the crystal. The parameters in (11) are calculated for room temperature (24 °C), a detailed temperature dependence is given in [48].

2.4.2 Induced noncolinear frequency doubling

Whereas SNCFD makes use of scattered light to provide the second fundamental wave, induced noncolinear frequency doubling (INCFD) takes two independent fundamental laser beams crossed inside the crystal to generate second harmonic light [49]. To achieve phase matching, either the geometry (i. e. the angle between the two fundamental beams) or the temperature can be used as tunable parameters. Calibration curves for c_{Li} as a function of the angle – at fixed temperature – or as a function of the temperature – at fixed angle – can be derived from the temperature dependent generalised Sellmeier equation [48]. As the interaction volume is limited in all three spatial dimensions, the method can be used for a sample characterisation with three-dimensional spatial resolution [50].

2.5 Holographic scattering

Based on the photorefractive effect, two laser beams inclined to each other can form a holographic grating in LiNbO_3 doped with photorefractive centers. The diffraction conditions for a fourth beam diffracted from a third incident beam depend on the refractive indices, thus on the composition of the material, when at least one of the interacting four beams differs in polarisation from the other ones. Arizmendi

[51] used an anisotropic diffraction arrangement where two extraordinary beams form a holographic grating, a third, weaker one is anisotropically diffracted into an ordinary one. Phase matching for this process must be achieved by angle tuning. The composition dependence of the phase matching condition can be calculated using the generalised Sellmeier equation [42]. Van Olfen et al. [52] showed that the necessary beams for the method can be generated by anisotropic scattering shining only one intense laser beam onto the sample. The experimental arrangement is much simpler as phase matching is achieved automatically without tuning any experimental parameter. The cone angle of the anisotropically scattered light is a measure for the composition.

2.6 Linewidth of Raman modes

Raman scattering was among the first calibration methods used for polycrystalline samples [53]. Compositional changes are observed not in the mode frequencies but in the damping. The damping is caused by a temperature-independent inhomogeneous part due to impurities and a temperature dependent homogeneous one due to anharmonicities of the interionic potentials. Thus the linewidths of certain modes have to be analysed. Kojima [54] investigated A_1 modes in backscattering geometry, because the contribution of Li or Nb to particular vibrational mode patterns was of interest, while Schlarb et al. [55] used the more convenient right angle scattering to correlate the composition to Raman mode halfwidths. For an unambiguous determination of the linewidth Γ the E -mode at 153 cm^{-1} and the A_1 mode at 876 cm^{-1} were chosen, because they show weak directional dispersion and do not overlap with other bands. A linear relation was found for both modes with the concentration in mol% and Γ in wavenumbers.

$$c_{\text{Li}} = 53.03 - 0.4739 \Gamma \quad \text{for the } 153\text{ cm}^{-1} \text{ phonon} \quad (12)$$

$$c_{\text{Li}} = 53.29 - 0.1837 \Gamma \quad \text{for the } 876\text{ cm}^{-1} \text{ phonon} \quad (13)$$

The estimated uncertainties in the Raman linewidths correspond to a compositional resolution of 0.05 mol%. Like other optical methods Raman scattering requires polished samples, but allows a small sample size.

2.7 Linewidth of OH stretch mode bands

Hydrogen is present in almost all LiNbO_3 crystals not specially treated after the growth process [56]. It forms with oxygen of the host an OH molecule with a distinct stretching vibration at about 3500 cm^{-1} . The corresponding absorption band, which is easily measured by high resolution infrared spectroscopy in small plates polished on two surfaces, is completely polarised perpendicular to the c -axis. Congruent samples show a broad non-symmetrical absorption band with a halfwidth of about 30 cm^{-1} [57]. With increasing Li in the bulk the broad band becomes more structured and a relatively sharp line at 3466 cm^{-1} emerges with the simultaneous decrease of the other components [58]. Close to the stoichiometric limit one is left with a single line at 3466 cm^{-1} with minor satellites [59]. Even these minor satellites are

diminished in numbers and intensity in a crystal recently grown in Budapest by K. Polgár. This sample exhibits a halfwidth of less than 3 cm^{-1} at room temperature, which is even smaller than that for VTE treated specimens [59]. In principle the halfwidth dependence seems to be suitable for calibration purposes, at least above 49.5 mol% Li_2O content. An alternative method for composition characterisation has recently been suggested by Kovács [60] using the intensity ratio of the band at 3466 cm^{-1} and the satellite at 3479 cm^{-1} . This ratio changes by at least two orders of magnitude in the 49.5 - 50 mol% range and would allow a composition determination with a relative accuracy of about 0.01 mol%. The weakness of both the halfwidth and the intensity ratio methods is that the shape of the OH band depends slightly on the impurities and the time passed since crystal growth or any heat treatments applied to the sample.

2.8 Luminescence measurements

Finally we briefly discuss the intrinsic luminescence in LiNbO_3 , which is strongly governed by the concentration of Li vacancies. For such measurements one usually needs samples of moderate size polished on three surfaces. Although the intensity of the UV-excited intrinsic luminescence at $T = 80\text{ K}$ varies linearly by at least two orders of magnitude [61] when going from a Li-deficient composition to an almost stoichiometric of 49.95 mol% Li_2O , this sensitivity is of no help for the determination of a crystal composition. As usually in emission spectroscopy, the major difficulty is caused by the intensity calibration, which in principle is possible but not a quick and easy task. In addition the sample geometry and the quality of the polished surfaces influence the result. Fischer et al. [61] reported that the spectral position of the luminescence maximum depends on the Li/Nb ratio. No calibration were given because of the low accuracy (approx. 0.2 mol%) of this method caused by the strongly varying bandshape.

3 Characterisation of the crystal homogeneity

All composition sensitive measurements which allow the investigation of spatially restricted volumina may be suitable to characterise the spatial homogeneity of the crystal. From the techniques discussed above mainly the various frequency doubling methods (see Sections 2.3 and 2.4) can be proposed.

Measurements of the phase matching temperature can be applied either working with a focussed laser beam and moving the crystal or illuminating the crystal uniformly and using a one- or two-dimensional detector array for detecting the generated second harmonic light [62]. Two-dimensional topographies are possible using this technique, the spatial resolution depends on the sample thickness and can be better than about $20\text{ }\mu\text{m}$ for thin platelets.

SNCFD measurements are excellently suited for homogeneity characterisations, such measurements can be carried out without varying the sample temperature, yet an automatic evaluation algorithm for the measured cones is necessary [47]. Again a two-dimensional spatial resolution is possible.

Table 2. List of methods discussed with a short characterization

Method	Properties	Accuracy (mol%)		Remarks
		abs.	rel.	
Chemical analysis	destructive, slow	0.2		several methods
Melt composition	qualitative			
Curie temperature	quantitative	0.1		recommended
Density	qualitative			
X-ray diffraction	quantitative	0.3-0.4		
Linewidth NMR, EPR	semi quantitative	0.1-0.25	0.05	low temperature
SAW velocity	qualitative	?	0.01	
Ion beam methods	qualitative			
UV absorption edge	quantitative, fast	0.1	0.02	recommended
Refractive index	quantitative	0.1	0.05	
Birefringence	quantitative, fast	0.1	0.01	recommended
SHG phase matching temperature	quantitative	0.1	0.01	recommended
SHG phase matching angle	quantitative, fast	0.2	0.02	
SNCFD	quantitative, fast	0.1	0.01	recommended
INCFD	quantitative	0.1	0.01	homogeneity test
Interferometry	quantitative		0.01	homogeneity test
Holographic scattering	quantitative	~ 0.1		only in photorefractive samples
Raman scattering	quantitative	0.1	0.05	
OH vibration	qualitative			
Luminescence	qualitative			

The only nondestructive technique which allows three-dimensional spatial resolution is – to our knowledge – induced noncolinear frequency doubling. The interaction volume is restricted in all three spatial dimensions, albeit the spatial resolution is not equally good in all three directions. In practice, one has to make a compromise between spatial and compositional resolution.

In addition to the described methods interferometric techniques can also be applied for homogeneity control, but only for samples having good optical quality [62]. Finally we mention spatially resolved Raman scattering but have to point out that the evaluation of the halfwidth is cumbersome or at least time consuming.

4 Conclusions

The described methods and their characteristic features are summarised in Table 2. Out of the quantitative methods eligible for the determination of the composition of lithium niobate crystals we sort out those which are non-destructive, accurate, fast, and easy to apply. Our survey shows that besides the measurement of the Curie temperature only some optical methods meet these requirements. One set of methods takes advantage of changes of the index of refraction. Although they use different experimental setups, they are linked by the generalised Sellmeyer equation introduced and explained above. A second candidate is the optical absorption at low absorption coefficients. All these methods allow an absolute accuracy of 0.1 mol% and a relative one of up to 0.01 mol%, a compositional resolution sufficient for most purposes and better than available so far.

As a rule impurities influence the properties of LiNbO₃ weaker than a similar concentration of missing Li ions. Thus the presence of background impurities can usually be neglected. For the Curie temperature and all refractive index based methods higher levels of certain impurities can explicitly be taken into account [63, 64].

Acknowledgements. The authors are grateful to the members of the Oxide Crystal Network whose opinions are summarised in the present work and to the ESF for promoting the Network's endeavours to arrive at broadly accepted standard methods in the field. They are also indebted to K. Polgár and E. Kokanyan (within INTAS-94-1080) for supplying them with samples, to G. Greten and L. Kovács for measuring the OH absorption band, and to G. Ruschhaupt, I. Földvári and A. Reichert for measurements of the absorption edge and/or the SHG. Part of this work was supported by Sonderforschungsbereich 225 'Oxidic crystals for electro- and magneto-optical applications', funded by DFG, and by the Hungarian Science and Research Fund (OTKA) under grant numbers T4110, T4367, and T4420.

References

1. A. Rüber: In *Current Topics in Materials Science*, ed. by Kaldis, Vol. 1 (North-Holland, Amsterdam 1978) p. 48
2. R. S. Weis, T. K. Gaylord: *Appl. Phys. A* **37**, 191 (1985)
3. O. F. Schirmer, O. Thiemann, M. Wöhlecke: *J. Phys. Chem. Solids* **52**, 185 (1991)
4. E. Krätzig, O. F. Schirmer: In *Photorefractive Materials and Their Applications*, Eds. P. Günter and J.P. Huignard, *Topics Appl. Phys.* Vol. 61, Springer, Berlin, Heidelberg 1988
5. M. Lawrence: *Reports on Progress in Phys.* **56**, 363 (1993)
6. D. R. Selviah: *MRS Bulletin*, March 1994, p. 50
7. P. Lerner, C. Legras, J. Dumas: *J. Cryst. Growth* **3-4**, 231 (1968)
8. L. O. Svaasand, M. E. Eriksrud, G. Nakken, A. P. Grande: *J. Cryst. Growth* **22**, 230 (1974)
9. S. Kan, M. Sakamoto, Y. Okana, K. Hoshikawa, T. Fukuda: *J. Cryst. Growth* **119**, 215 (1992)
10. K. Kitamura, J. K. Yamamoto, N. Iyi, S. Kimura, T. Hayashi: *J. Cryst. Growth* **116**, 327 (1992)
11. Y. S. Luh, M. M. Fejer, R. L. Byer, R. S. Feigelson: *J. Cryst. Growth* **85**, 264 (1987)
12. N. Iyi, K. Kitamura, F. Izumi, J. K. Yamamoto, T. Hayashi, H. Asano, S. Kimura: *J. Sol. State Chem.* **101**, 340 (1992)
13. R. L. Holman: *Mater. Sci. Res.* **11**, 343 (1978)
14. D. H. Jundt, M. M. Fejer, R. L. Byer: *IEEE J. Quantum Electron.* **26**, 135 (1990)
15. G. I. Malovichko, V. G. Grachev, L. P. Yurchenko, V. Y. Proshko, E. P. Kokanyan, V. T. Gabrielyan: *phys. stat. sol. (a)* **133**, K29 (1992)
16. G. I. Malovichko, V. G. Grachev, E. P. Kokanyan, O. F. Schirmer, K. Betzler, B. Gather, F. Jermann, S. Klauer, U. Schlarb, M. Wöhlecke: *Appl. Phys. A* **56**, 103 (1993)

17. G.-Guo Zhong, J. Jian, Z.-Kong Wu, Proc. 11th Intern. Quantum Electronics Conf., June, 1980, IEEE Cat. No. 80, CH-1561-0, p. 631
18. T. Volk, N. Rubinina, V. Pryalkin: Opt. Lett. **15**, 996 (1990)
19. T. Volk, M. Wöhlecke, N. Rubinina, N. V. Razumovski, F. Jermann, C. Fischer, R. Böwer: Appl. Phys. A **60**, 217 (1995)
20. J. C. Yamamoto, K. Kitamura, N. Iyi, S. Kimura, Y. Furukawa, M. Sato: Appl. Phys. Lett. **61**, 2156 (1992)
21. B. Grabmaier, F. Otto: J. Cryst Growth **79**, 682 (1986)
22. Y. Furukawa, M. Sato, K. Kitamura, Y. Yajima, M. Minakata: J. Appl. Phys. **72**, 3250 (1992)
23. Polgár, L. Jeszenszky, K. Raksányi, E. Hartmann: Acta Phys. Hung. **47**, 125 (1979)
24. J. R. Carruthers, G. E. Peterson, M. Grasso, P. M. Bridenbaugh: J. Appl. Phys. **42**, 1846 (1971)
25. U. Schlarb: Dissertation, Shaker (1994), ISBN 3-8265-0097-0, p. 69 ff.
26. P. F. Bordui, R. G. Norwood, D. H. Jundt, M. M. Fejer: J. Appl. Phys. **71**, 875 (1992)
27. P. F. Bordui, R. G. Norwood, C. D. Bird, G. D. Calvert: J. Crystal Growth **113**, 61 (1991)
28. H. M. O'Bryan, P. K. Gallagher, C. D. Brandle: J. Am. Ceram. Soc. **68**, 493 (1985)
29. B. Guenais, M. Baudet, M. Minier, M. LeCun: Mater. Res. Bull. **16**, 643 (1981)
30. P. K. Gallagher, H. M. O'Bryan, Jr.: J. Am. Ceram. Soc. **68**, 147 (1985)
31. B. C. Grabmaier, W. Wersing, W. Koestler: J. Cryst Growth **110**, 339 (1991)
32. L. Kovács, K. Polgár: Cryst. Res. Techn. **21**, K101 (1986)
33. S. C. Abrahams, P. Marsh: Acta Cryst. B **42**, 61 (1986)
34. N. Zotov, H. Boysen, F. Frey, T. Metzger, E. Born: J. Phys. Chem. Solids, **55**, 145 (1994)
35. G. I. Malovichko, O. Cerclier, J. Estienne, V. G. Grachev, E. P. Kokanyan, C. Boulesteix: J. Phys. Chem. Solids **56**, 1285 (1995)
36. G. E. Petersen, J. R. Carruthers: J. Solid State Chem. **1**, 98 (1969)
37. J. Blümel, E. Born, T. H. Metzger: J. Phys. Chem. Solids **55**, 589 (1994)
38. G. I. Malovichko, V. G. Grachev, O. F. Schirmer: Solid State Commun. **89**, 195 (1994)
39. J. Kushibiki, H. Takahashi, T. Kobayashi, N. Chubachi: Appl. Phys. Lett. **58**, 2622 (1991)
40. K. Yamada, H. Takemura, Y. Inoue et al.: Japan. J. Appl. Phys. **26**, Suppl. 26-2, 219 (1987)
41. I. Földvári, K. Polgár, R. Voszka, R. N. Balasanyan: Crystal Res. Technol. **19**, 1659 (1984)
42. U. Schlarb, K. Betzler: J. Appl. Phys. **73**, 3472 (1993).
43. U. Schlarb, K. Betzler: Phys. Rev. **B48**, 15613 (1993)
44. N. Schmidt, K. Betzler, B. C. Grabmaier, Appl. Phys. Lett. **58**, 34 (1991).
45. R. L. Byer, J. F. Young, R. S. Feigelson, J. Appl. Phys. **41**, 2320 (1970).
46. A. Reichert, K. Betzler: Ferroelectrics **126**, 9 (1992)
47. A. Reichert, K. U. Kasemir, K. Betzler: Ferroelectrics, in print (1996)
48. U. Schlarb, K. Betzler: Ferroelectrics **156**, 99 (1994)
49. A. Reichert, K. Betzler: Ferroelectrics, **156**, 93 (1994)
50. A. Reichert, K. Betzler: J. Appl. Phys. **79** (15 February 1996)
51. L. Arizmendi: J. Appl. Phys. **64**, 4654 (1988)
52. U. van Olfen, R. A. Rupp, E. Krätzig, B. C. Grabmaier: Ferroelectrics Letters **10**, 133 (1989)
53. A. E. Balanevskaya, L. I. Pyatigorskaya, Z. I. Shapiro, L. N. Margolin, and E. A. Bovina, J. Appl. Spectrosc. **38**, 491 (1983)
54. S. Kojima: Jpn. J. Appl. Phys. **32**, 4373 (1993)
55. U. Schlarb, S. Klauer, M. Wesselmann, K. Betzler, M. Wöhlecke: Appl. Phys. A **56**, 311 (1993)
56. R. González, E. R. Hodgson, C. Ballesteros, Y. Chen: Phys. Rev. Lett. **15**, 2057 (1991)
57. J. H. Herrington, B. Dischler, A. Räuber, J. Schneider: Solid State Commun. **12**, 351 (1973)
58. L. Kovács, V. Szalay, R. Capelletti: Solid State Commun. **52**, 1029 (1984)
59. A. Gröne, S. Kapphan: J. Phys. Chem. Solids **56**, 687 (1995)
60. L. Kovács, private communication
61. C. Fischer, M. Wöhlecke, T. Volk, N. Rubinina: phys. stat. sol. (a) **137**, 247 (1993)
62. N. Schmidt, K. Betzler, S. Kapphan: Cryst. Latt. Def. and Amorph. Mat. **15**, 103 (1987).
63. U. Schlarb, M. Wöhlecke, B. Gather, A. Reichert, K. Betzler, T. Volk, N. Rubinina: Optical Materials **4**, 791 (1995).
64. U. Schlarb, B. Matzas, A. Reichert, K. Betzler, M. Wöhlecke, B. Gather, T. Volk: Ferroelectrics, in print (1996).

This article was processed by the author using the L^AT_EX style file *pljour2* from Springer-Verlag.